

Investigation of the Threshold Level of H₂S for Pitting of Mild Steel in CO₂ Aqueous Solutions

Wei Yan, Bruce Brown*, Srdjan Nesic

Institute for Corrosion and Multiphase Technology, Ohio University, Athens, OH 45701, USA

*Corresponding author: brownb1@ohio.edu

ABSTRACT

A series of experiments was conducted in a large-scale multi-phase flow loop to investigate the threshold level of H₂S leading to localized attack on mild steel in CO₂ saturated aqueous solution with 1% wt NaCl at 40°C. The CO₂ partial pressure was fixed at 8.0 bar in all test conditions and the H₂S partial pressure was varied from 0.024mbar (3ppm) to 0.5mbar (60 ppm). The superficial liquid velocity was 0.8 m/s and the experiment duration was between 2 and 21 days. The experimental results revealed that when the H₂S partial pressure was low and the saturation value for mackinawite was near unity, localized attack occurred. Using the methodology provided, the corrosion behavior in very low pH₂S environments may be predicted according to the super saturation levels of mackinawite.

Keywords: low H₂S corrosion; localized attack; threshold value; mild steel

INTRODUCTION

The type of corrosion observed inside upstream oil and gas production pipelines is, among other variables, related to the chemistry of the water phase, which is directly influenced by the partial pressures of the acid gases, CO₂ and H₂S. These gases are present in many oil and gas reservoirs in varying concentrations and concentration ratios. Over the last decade, research has shown that small amounts of H₂S can retard the general CO₂ corrosion rate of carbon steel¹⁻¹¹. However, the possibility of localized corrosion due to small amounts of H₂S has not been addressed until recently¹²⁻¹⁶. The main reason for the retardation of the general corrosion rate is the rapid formation of a moderately protective iron sulfide layer¹⁰, which has been found to be mackinawite. Mackinawite is the first iron sulfide to form when mild steel is exposed to [H₂S]_{aq}, but many types of other iron sulfides may also form with time, depending on environmental conditions, such as cubic ferrous sulfide, smythite, greigite, troilite, pyrrhotite, and pyrite^{4, 17}. It has been observed that transition from mackinawite to the other forms of iron sulfide may lead to localized corrosion¹⁸⁻²⁰, but this is expected to occur at high partial pressures of H₂S. At the very low partial pressures, mackinawite has been found to be the dominant iron sulfide corrosion product⁴. It is hypothesized that at some very low H₂S concentrations, the protective properties of the mackinawite layer will be compromised, leading to localized corrosion. This study presents an initial investigation of the threshold value of pH₂S leading to initiation of localized corrosion under high pressure multiphase flow conditions.

EXPERIMENTAL

Equipment

All experiments in this study were conducted in a 2000-liter Hydrogen Sulfide Multiphase Flow Loop depicted in **Figure 1**. The experimental equipment has been described fully in an earlier publication²¹. Experimental parameters, such as pH, temperature, total pressure, and iron concentration, were measured prior to the insertion of flush mounted mild steel electrochemical probe and weight loss (WL) specimens, and each parameter was monitored throughout each experiment. Experiments lasted from 2 days to 21 days.

H₂S concentration in the gas phase was measured with a GASTEC[†] model GV-100S piston pump using low range standard detection tubes with a range from 1 to 240 ppm to measure an effluent gas stream at atmospheric conditions. The length of color change in the reagent detection tube was measured using calipers to increase the accuracy of the value. Repeatability of this method was found to be $\pm 5\%$.

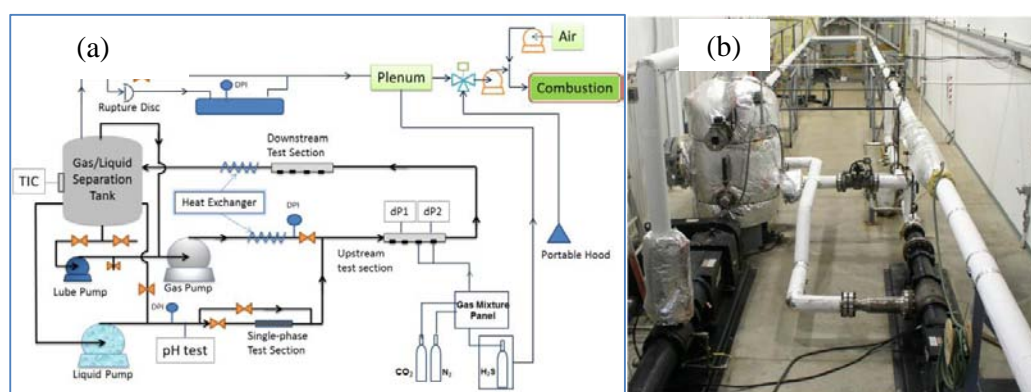


Figure 1 Large scale H₂S Multiphase Flow Loop (a) schematic (b) image

Instrumentation

A three-electrode electrochemical method was used to monitor the trend in corrosion rate, using a nickel 200 probe as a reference electrode, an API 5L X65 mild steel probe as the working electrode and the Hastelloy C-276 piping as the counter electrode. Linear polarization resistance (LPR), measured with a Gamry[‡] Reference 600 potentiostat, was used to determine general corrosion rate once per day (only for the first test). A Thermo Scientific GENESYS[§] 10vis spectrophotometer at 510 nm wavelength was used with specific procedures to determine the Fe²⁺ concentration from 10ml liquid samples collected during each experiment. Scanning electron microscopy (SEM) and energy dispersive spectroscopy (EDS) were used to analyze the corrosion product layer and an Alicona^{**} infinite focus microscope was the high resolution profilometer used to analyze the specimen surface topography after removing the corrosion product layer.

[†] Trade Name

[‡] Trade Name

[§] Trade Name

^{**} Trade Name

Material

The API 5L X65 mild steel used in this experimental study has the chemical composition shown in **Table 1**.

Table 1
Chemical composition of API 5L X65 mild steel (mass %)

C	Mn	Si	P	S	Cr	Mo	Ni	Al	Cu	Fe
0.13	1.16	0.26	0.009	0.009	0.14	0.16	0.36	0.032	0.13	balance

Test Matrix

Three long-term experiments were conducted in this study as shown in the test matrix (**Table 2**). Temperature, CO₂ partial pressure, liquid velocity, gas velocity and NaCl content were not varied. H₂S partial pressure, pH, and exposure time varied in the three experiments.

Table 2
Test Matrix

Parameters	Test 1	Test 2	Test 3
Solution		1 wt% NaCl	
Temperature		40°C ±1°C	
CO ₂ partial pressure		8.0 bar	
Total pressure		8.07 bar	
Superficial liquid velocity (V_{sl})		0.8 m/s	
Superficial gas velocity (V_{sg})		4.0 m/s	
Dissolved oxygen		< 10 ppb	
Dissolved iron		As measured	
H ₂ S concentration (partial pressure)	None added, increased spontaneously	3 ppm (0.024mbar)	60 ppm (0.5mbar)
pH	as measured	pH 4.7±0.2	pH 4.7±0.2
Weight loss specimen exposure time	5, 7, 15 and 21 days	2 days	7 days and 21 days

Procedure

All experiments performed in this large-scale multiphase flow loop were done by using the following procedure:

- Rinse flow loop with tap water, then with deionized water (DI water) 2-3 times.
- Add 350 gal (1325L) DI water and 1% wt NaCl to the tank.
- Purge the system with CO₂ gas. During the purging process, both pumps running at a low flow rate and temperature set 40°C.
- When measured O₂ concentration was lower than 10 ppb, gas purging stopped and total pressure increased with CO₂ to 8.07 bar (117 psi).

- e) Set the two pumps rotation speed for the designated flow rate.
- f) Record the pressure, pH, and Fe^{2+} concentration.
- g) Add pure H_2S as needed, wait $\frac{1}{2}$ hour before measurement.
- h) Measure concentration of H_2S in the gas phase effluent at ambient pressure.
- i) Once operating parameters are stable, insert weight loss specimen and electrochemical probes flush mounted into the loop.
- j) Retrieve WL specimen at predetermined times for analysis; rinse them with deoxygenated DI water to remove salts and deoxygenated isopropanol to remove water to minimize the damage to the corrosion product layer. After drying, the specimen weight was recorded, and a digital photograph recorded. All specimens were stored in a vacuum desiccator prior to the analysis.

In normal operation of the large scale H_2S flow loop, it has been observed that residual amounts of H_2S may be found in subsequent experiments at much lower concentrations than used in the previous experiment, even after thorough cleaning procedures have been followed. This is due to absorption of H_2S by the plastic and elastomer components in the system. The first experiment reviewed below was conducted at nominally zero concentration of H_2S (no H_2S was added) however a very low H_2S concentration was recorded, that increased with time, as explained below.

RESULTS AND DISCUSSION

The first experiment in this study was used to identify the influence of varied low partial pressures of H_2S on the type of corrosion observed. The more controlled second and third experiments were used to confirm the initial observations.

Initial Testing (Experiment 1)

Figure 2 shows the pH and iron concentration change with time during the first experiment. The bulk solution pH increased slightly from pH 4.4 to pH 4.9 over 21 days; the measured ferrous ion concentration changed from 86 mg/L to 259 mg/L during the test. Even if no H_2S was added, the final H_2S content was 0.96 mbar (120 ppm). Measurements showed that H_2S partial pressure increased almost linearly with time. Six WL specimens were used in this experiment, retrieved at different times, all experiencing slightly different conditions, as shown in Table 3.

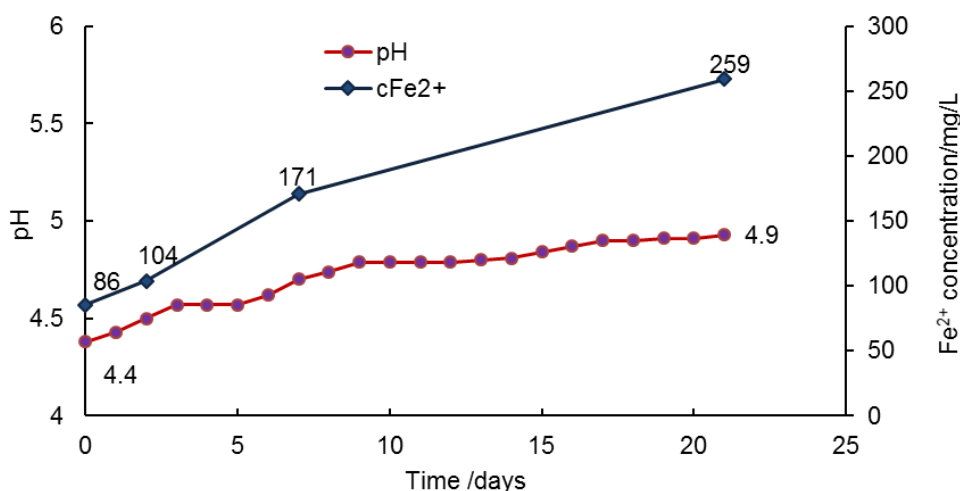


Figure 2 Experiment 1: pH and $[\text{Fe}^{2+}]$ vs. time. 1 wt% NaCl solution, 40°C , 8 bar pCO_2 , $V_{\text{sl}} = 0.8$ m/s, $V_{\text{sg}} = 4.0$ m/s, 0 - 120 ppm $\text{H}_2\text{S}/\text{CO}_2$

Table 3
WL Specimen experimental test parameters

Specimen No.	Duration	Exposure Time, days	Start: initial pH ₂ S / mbar (ppm H ₂ S/CO ₂)	End: final pH ₂ S / mbar (ppm H ₂ S/CO ₂)
1	From 0 to 7 days	7	0.03 (3)	0.25 (30)
3	From 0 to 21 days	21	0.03 (3)	0.68 (85)
4	From 0 to 21 days	21	0.03 (3)	0.68 (85)
5	From 7 to 22 days	15	0.25 (30)	0.71 (90)
6	From 21 to 26 days	5	0.68 (85)	0.84 (100)

The corrosion rates measured by LPR and WL are shown in **Figure 3**. The B value for the LPR calculation was taken as 26 mV. The LPR corrosion rates represent a trend in the corrosion rate of the system and show a decreasing rate as a protective corrosion product layer developed. The WL measurements are based on the total (integral) mass loss for each specimen.

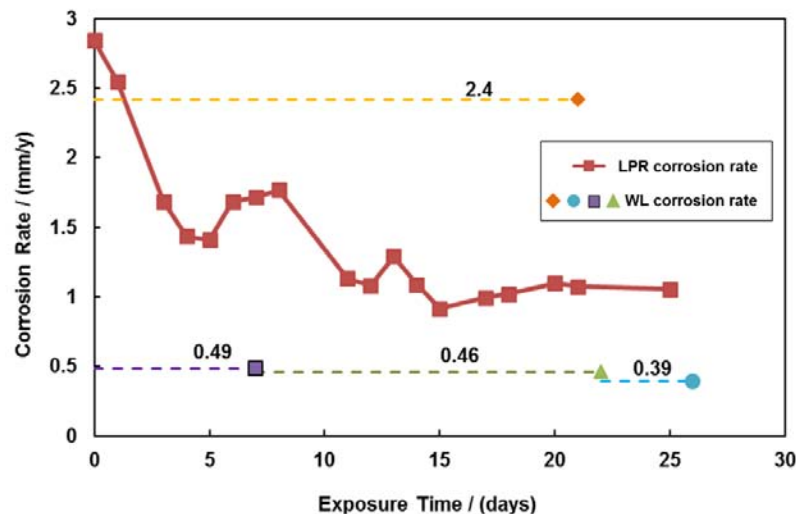


Figure 3 Experiment 1: general corrosion rates from LPR and WL measurements vs. time. 1 wt% NaCl solution, 40°C, 8 bar pCO₂, V_{sl} = 0.8 m/s, V_{sg} = 4.0 m/s, 0 - 120 ppm H₂S/CO₂

Surface morphology images of the corrosion products layer are shown in **Figure 4** and the images and morphology of the metal surface without the corrosion product for each specimen is shown in **Figure 5**. The WL specimen that were exposed from the beginning of the experiment (**Figure 4 (a) and (b)**) experienced very low pH₂S in the range of 0.03 to 0.25 mbar H₂S (3 to 30 ppm H₂S/CO₂) and both had severely damaged corrosion product layers with cracks or holes observed. After removing the corrosion product layer with Clarke solution²², profilometry found severe localized corrosion attack with pit penetration rates of 11.1 mm/y and 10.6 mm/y respectively. Based on ASTM G46²³, both can be said to suffer from pitting corrosion. Surface of the WL specimen exposed from Day 7 to Day 22 experienced higher partial pressures of H₂S, in the range of 0.25 mbar to 0.7 mbar (30 to 90 ppm H₂S/CO₂), and are shown in **Figure 4 (c)** and **Figure 5 (c)**. The corrosion product layer seems to be more uniform, but some small defects can be observed on the surface. After removing the scale and performing profilometry, pitting corrosion was observed, with a maximum measured pit penetration rate of 3.7 mm/y. The analysis of the

WL specimen that was exposed for 5 days near the end of the experiment (day 21 to day 26) at the highest partial pressures of H₂S, in the range of 0.68 to 0.84 mbar (85 to 100 ppm H₂S/CO₂) is shown in **Figure 4 (d)** with profilometry analysis shown in **Figure 5 (d)**. The corrosion product on the surface of this specimen looks uniform with no defects (cracks or holes), as well as no localized corrosion observed after removing the corrosion product layer.

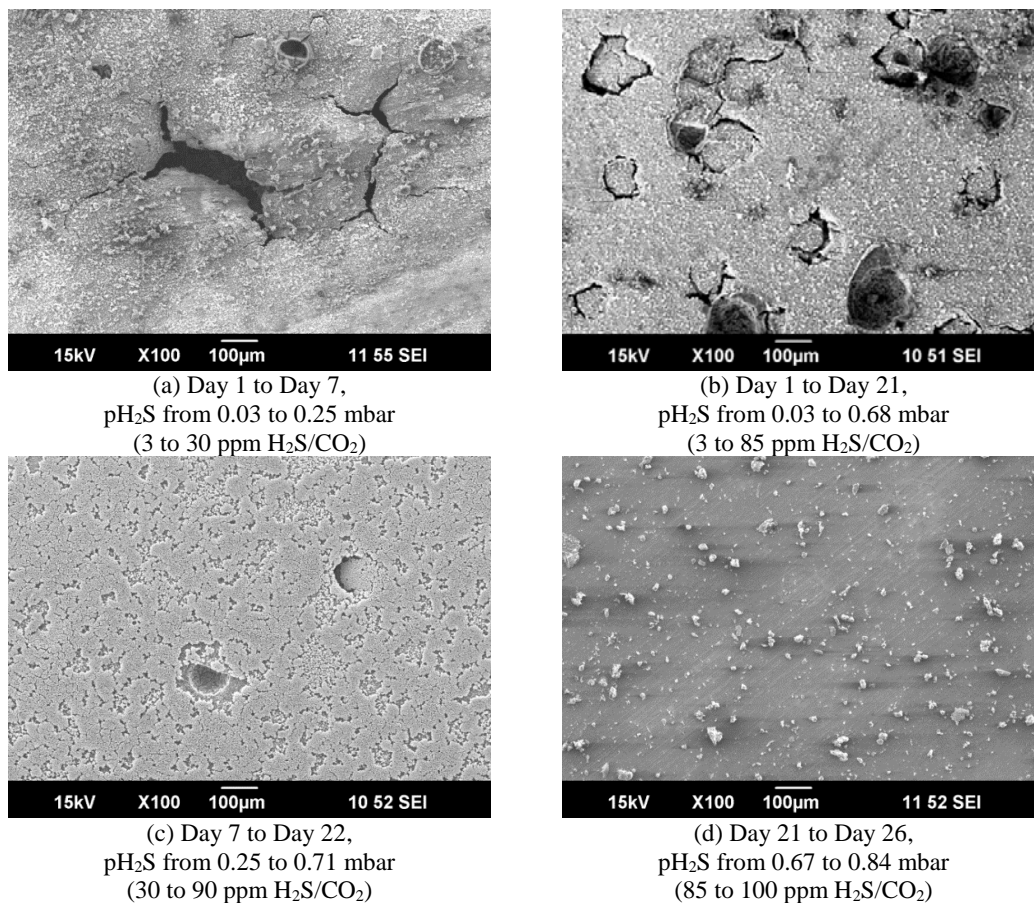


Figure 4. Experiment 1: comparison of corrosion product layer for WL specimen exposed to varied pH₂S. (a) 7 days; (b) 21 days; (c) 15 days; (d) 5 days. 1 wt% NaCl solution, 40°C, 8 bar pCO₂, V_{sl} = 0.8 m/s, V_{sg} = 4.0 m/s, 0 - 120 ppm H₂S/CO₂

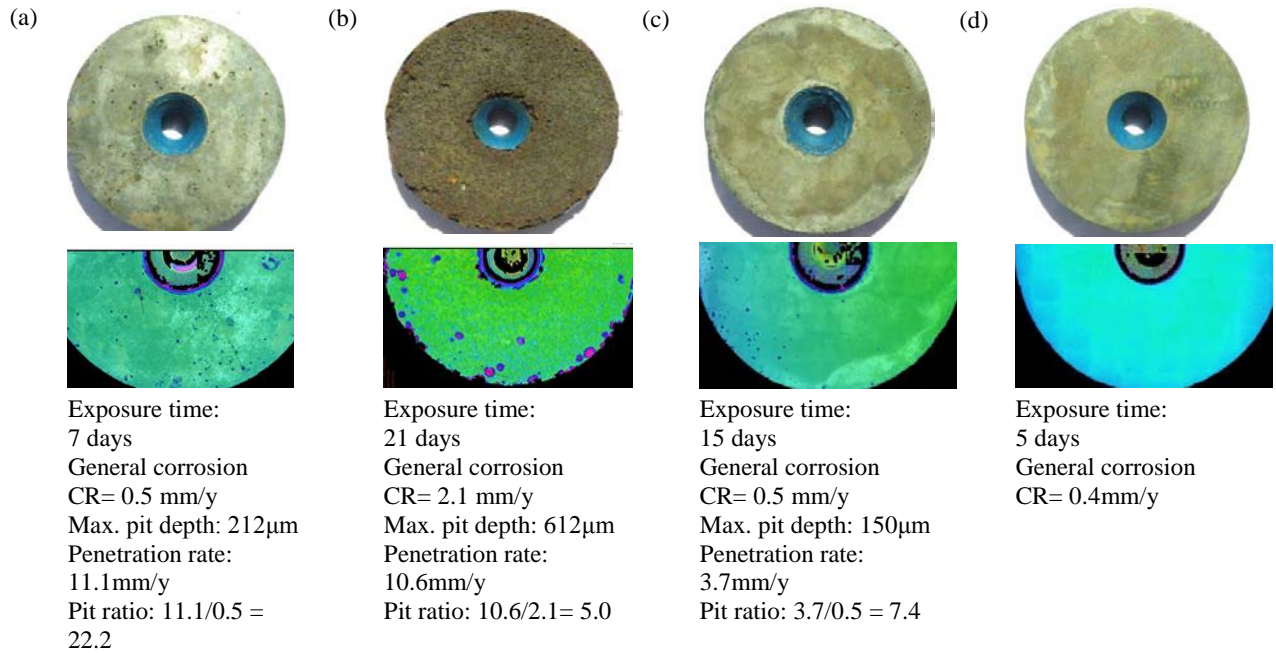


Figure 5. Experiment 1: surface features and profilometry of the surface after removing the corrosion product layer. (a) 7 days; (b) 21 days; (c) 15 days; (d) 5 days. 1 wt% NaCl solution, 40°C, 8 bar pCO₂, V_{sl} = 0.8 m/s, V_{sg} = 4.0 m/s, 0 - 120 ppm H₂S/CO₂

The summary of these findings is given by plotting the maximum pit penetration rates vs. H₂S partial pressure in **Figure 6**.

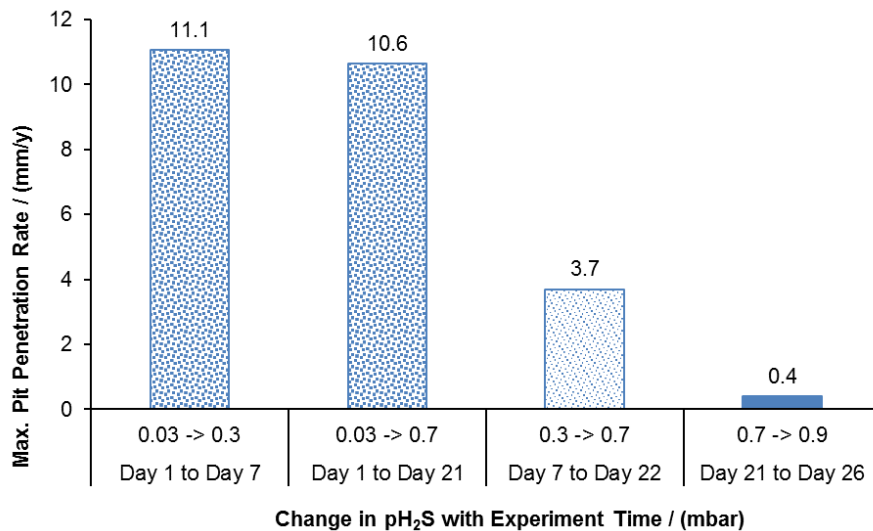


Figure 6. Experiment 1: comparison of maximum pit penetration rates vs. the variation of H₂S partial pressure during the experiment. 1 wt% NaCl solution, 40°C, 8 bar pCO₂, V_{sl} = 0.8 m/s, V_{sg} = 4.0 m/s, 0 - 120 ppm H₂S/CO₂

FeS Saturation Analysis

The corrosion rate retardation observed in Experiment 1 was caused by the protective mackinawite layer, which forms very fast on the steel surface. The solubility limit of mackinawite based on the concentration of the bisulfide ion (K_{sp,HS^-})²⁴ can be determined from the equilibrium expression for following reaction:



The saturation level of FeS_{mack} can be expressed as:

$$S_{FeS_{mack}} = \frac{[Fe^{2+}][HS^-]}{[H^+]K_{sp,HS^-}} \quad (2)$$

At saturation, where $S_{FeS_{mack}} = 1$, Equation (2) relates the bisulfide concentration to proton concentration:

$$[HS^-] = \frac{K_{sp,HS^-}}{[Fe^{2+}]} [H^+] \quad (3)$$

In order to find the bisulfide concentration, the dissociation step for aqueous H_2S needs to be considered:



where

$$K_{a,1} = \frac{[H^+][HS^-]}{[H_2S]} \quad (5)$$

The aqueous concentration of H_2S is calculated from the gas/liquid equilibrium reaction for H_2S ²⁵,



where

$$K_{H_2S,sol} = \frac{[H_2S]}{pH_2S} \quad (7)$$

By substitution of Equation (3) and Equation (7) into Equation (5) for $[HS^-]$ and $[H_2S]$, respectively, the relationship between H_2S partial pressure and saturation H^+ concentration can be expressed by:

$$p_{H_2S}(K_{H_2S}K_{a,1}) = \frac{K_{sp,HS^-}}{[Fe^{2+}]} [H^+]^2 \quad (8)$$

Rearranging Equation (8), an H_2S partial pressure leading exactly to saturation of mackinawite ($S_{FeS_{mack}} = 1$) can be determined as a function of solution pH:

$$p_{H_2S} = \left[\frac{K_{sp,HS^-}}{K_{H_2S}K_{a,1}[Fe^{2+}]} \right] (10^{-pH})^2 \quad (9)$$

where each of the reaction constants are a function of temperature:

$$K_{H_2S,sol} = 10^{(-0.71742672-0.012145427T_c+5.6659982 \times 10^{-5}T_c^2-8.1902716 \times 10^{-8}T_c^3)} \quad (10)^{26}$$

$$K_{a,1} = 10^{(782.43945+0.361261T_K-1.6722 \times 10^{-4}T_K^2-\frac{20565.7315}{T_K}-142.741722 \ln(T_K))} \quad (11)^{27}$$

$$K_{sp,HS^-} = 10^{\left(\frac{2848.779}{T_K}-6.347-\log(K_{a,1})\right)} \quad (12)^{27}$$

FeCO₃ Saturation

Although a corrosion product layer has been observed to be dominated by iron sulfide⁴ in environmental test conditions similar to the operating conditions shown in Table 2, iron carbonate (FeCO₃) has been shown to provide a protective corrosion product layer under some sweet corrosion conditions and should not be ignored. The equation for iron carbonate formation is shown as:



And the saturation level of FeCO₃ can be expressed as:

$$S_{FeCO_3} = \frac{[Fe^{2+}][CO_3^{2-}]}{K_{sp,FeCO_3}} \quad (14)$$

Where the reaction rate constant is a function of temperature (T_K) and ionic strength (I):

$$K_{sp,FeCO_3} = 10^{(-59.3498+0.041337 \cdot T_K-2.1963/T_K+24.5724 \cdot \log_{10} T_K+2.518 \cdot I^{0.5}-0.657 \cdot I)} \quad (15)^{31, 32}$$

By solving a set of equilibrium constant equations (a comprehensive list is given elsewhere²⁵) for the bicarbonate anion in terms the partial pressure of CO₂:

$$[CO_3^{2-}] = \left(\frac{K_{bi}K_{ca}K_{hy}K_{sol}}{[H^+]^2} \right) pCO_2 \quad (16)$$

This can be substituted into Equation (14), to derive an equation similar to Equation (9) for p_{H₂S}.

$$pCO_2 = \left[\frac{K_{sp,FeCO_3}}{K_{bi}K_{ca}K_{hy}K_{sol}[Fe^{2+}]} \right] (10^{-pH})^2 \quad (17)$$

Where each of the reaction constants is a function of temperature in Fahrenheit and ionic strength (I):

$$K_{bi} = 10^{-(10.61-4.97 \times 10^{-3}T_f+1.331 \times 10^{-5}T_f^2-2.624 \times 10^{-5}pCO_2-1.166\sqrt{I}+0.3466(I))} \quad (18)$$

$$K_{ca} = 387.6 \times 10^{-(6.41-1.594 \times 10^{-3}T_f+3.52 \times 10^{-6}T_f^2-3.07 \times 10^{-5}pCO_2-0.4772\sqrt{I}+0.1180(I))} \quad (19)$$

$$K_{hy} = 2.58 \times 10^{-3} \quad (20)$$

$$K_{sol} = \frac{14.5}{1.00258} \times 10^{-(2.27+5.65 \times 10^{-3}T_f - 8.06 \times 10^{-6}T_f^2 + 0.075(1))} \quad (21)$$

Surface Conditions vs. Bulk Solution Conditions

The corrosion rate of mild steel in an H₂S/CO₂ environment is affected by the partial pressure of H₂S, partial pressure of CO₂, temperature, solution pH, ionic strength, and flow velocity, which all also influence the corrosion product layer that forms (a more detailed description is provided elsewhere¹⁶). In addition, the corrosion product layer is also dependent upon the ferrous ion concentration, which is shown by Equation (2) and Equation (13) to be directly related to the saturation value. At the metal surface, where protons are consumed and ferrous ions are released by corrosion, this changes the solution composition. Experimentation has shown that the pH can increase at the metal surface up to 1 or even 2 pH units as compared to the bulk solution pH²⁸. By using this information, the saturation value at the metal surface can be estimated. In the conditions tested, the S(FeCO₃) in the bulk solution varied from under-saturated to super-saturated, while the S(FeS) was always under-saturated in the bulk solution. At the metal surface, it was estimated that the S(FeCO₃) was always super-saturated, while the S(FeS) varied from being slightly saturated to super-saturated. Analysis of the test specimen by SEM/EDS confirmed the corrosion product in each experiment to be dominated by iron sulfide, so the S(FeS_{mack}) values were correlated with the observations of localized corrosion.

It can be proposed that:

- 1) When the bulk solution was highly under-saturated with respect to FeS ($S_{FeS_{mack}} \ll 1$), while the surface solution is estimated to have slightly exceeded saturation with respect to FeS ($S_{FeS_{mack}} > 1$) – this resulted in partial coverage by protective FeS and severe pitting attack occurred;
- 2) When the bulk solution was under-saturated with respect to FeS ($S_{FeS_{mack}} < 1$) while the surface was estimated to be super-saturated with FeS ($S_{FeS_{mack}} \gg 1$) - full coverage by FeS was the result, and general corrosion was observed - without localized attack.

Corrosion Behavior Prediction (Experiment 2 and 3)

Results from Experiment 1 indicated the conditions where localized corrosion can be observed, but some of the crucial parameters, such as partial pressure of H₂S and pH were not stable and changed without proper control during the experiment. It is understood that variations in operating parameters during an experiment make it harder to determine the true cause and effect when trying to understand corrosion mechanisms, so these needed to be better controlled. For this reason, two additional controlled experiments were designed and carried out. The basic parameters for these two additional experiments are listed in **Table 2** with more details in **Table 4**, including whether or not localized corrosion should be expected based on $S_{FeS_{mack}}$. The measured ferrous ion concentration for these experiments was nominally 80mg/l (70 – 90 mg/l) and 250 mg/l (200 – 300 mg/l) respectively for Experiment 2 and Experiment 3.

Table 4
Conditions for S_{FeS} Calculation in Experiment 2 and 3.

Environmental Condition	Bulk pH	pH ₂ S mbar (ppm H ₂ S/CO ₂)	cFe ²⁺ (ppm(w))	Test Time (day)	Pitting Corrosion Expected?
Experiment 2	4.6	0.03 (3)	80	2	Yes
Experiment 3	4.8	0.5 (60)	250	21	No

The steel surface solution conditions of Experiment 2 were calculated to be slightly saturated with respect to FeS_{mack} and pitting attack was expected. The steel surface solution conditions of Experiment 3 were calculated to be super-saturated with respect to FeS_{mack} and general corrosion was expected with no localized attack.

Obtained measurements and surface morphologies confirmed these predictions. In Experiment 2, some pitting was found even after a very short exposure, while in Experiment 3, the two WL corrosion specimen removed after 7 days and after 21 days show uniform corrosion product layers (**Figure 7 (c) and (d)**). After the corrosion products were removed and the surface analyzed by the profilometer, no pitting was found on these specimen (**Figure 8 (b) and (c)**).

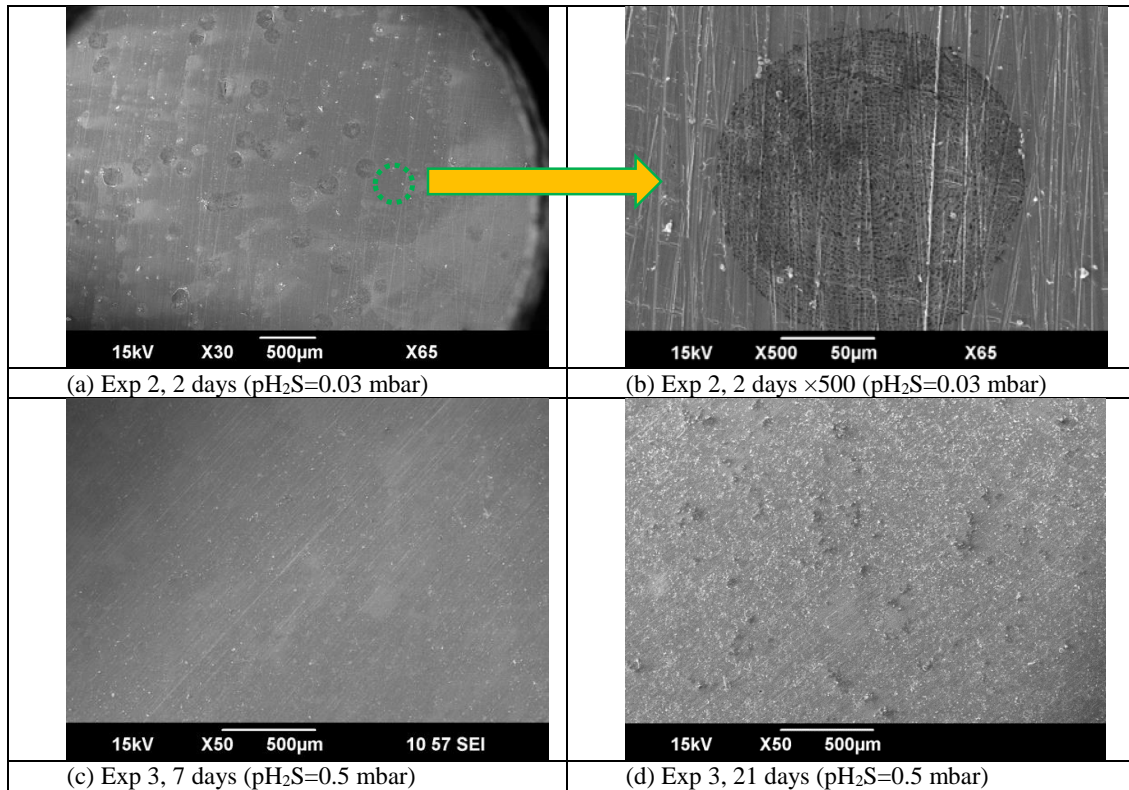


Figure 7. Comparison of corrosion product SEM images of Exp 2 and Exp 3. (a)Exp 2, 2days, 3 ppm H₂S/CO₂; (b) Exp 2, 2days, 3 ppm H₂S/CO₂; (c)Exp 3, 7days, 6 ppm H₂S/CO₂; (d) Exp 3, 21days, 6 ppm H₂S/CO₂. 1 wt% NaCl solution, 40°C, 8 bar pCO₂, V_{sl} = 0.8 m/s, V_{sg} = 4.0 m/s.

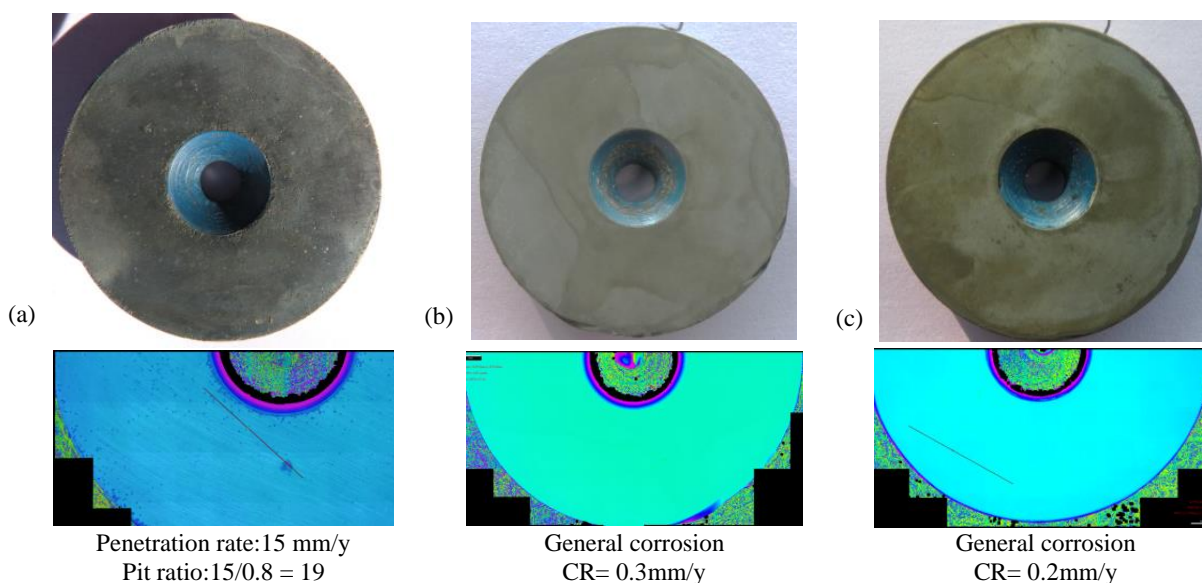


Figure 8. Profilometry analysis after removing corrosion products. (a) Exp 2, 2days, 3 ppm H₂S/CO₂; (b) Exp 3, 7days, 6 ppm H₂S/CO₂; (c)Exp 3, 21days, 6 ppm H₂S/CO₂; 1 wt% NaCl solution, 40°C, 8 bar pCO₂, V_{sl} = 0.8 m/s, V_{sg} = 4.0 m/s.

CONCLUSIONS

Three large scale corrosion experiments were conducted in a multiphase flow loop in order to investigate the value of threshold pH₂S leading to retardation of mild steel localized attack in CO₂ saturated solution. It was found that:

- (1) The threshold pH₂S is related to water chemistry and the saturation level of FeS_{mack}. Below this threshold, the [H₂S]_{aq} concentration at the steel surface is very low, leading to a slightly super-saturated solution and only a partial surface coverage by protective FeS_{mack}, resulting in localized attack on mild steel.
- (2) When the threshold pH₂S is exceeded and the surface saturation level of FeS_{mack} is higher (super-saturated solution) no localized corrosion was seen.
- (3) The actual threshold value of pH₂S is affected by water chemistry and mass transfer conditions of the system (ie. pCO₂, flow regime, flow rate, bulk solution pH, etc.). Therefore, no general value of pH₂S can be defined as a threshold value for localized corrosion since calculations are necessary to determine the steel surface water chemistry.

ACKNOWLEDGEMENTS

The authors would like to thank the following companies for their financial support: BP, Champion Technologies, Chevron, Clariant Oil Services, ConocoPhillips, DNV GL, ExxonMobil, Hess, INPEX Corporation, MI-SWACO, Multi-Chem, NALCO Energy Services, Occidental Oil Company, Petrobras, PETRONAS, PTT, Saudi Aramco, Total, TransCanada Pipelines, Ltd., and WGIM.

REFERENCES

1. B. Brown, S. R. Parakala, and S. Nestic, "CO₂ Corrosion in the Presence of Trace Amounts of H₂S," in *Corrosion/2004*, 2004, no. 04736, pp. 1–28.
2. E. Abelev, T. Ramanarayanan, and S. L. Bernasek, "Iron Corrosion in CO₂ Brine at Low H₂S Concentrations: An Electrochemical and Surface Science Study," *Journal of The Electrochemical Society*, vol. 156, no. 9, p. C331, 2009.

3. J. Tang, Y. Shao, J. Guo, T. Zhang, G. Meng, and F. Wang, "The effect of H₂S concentration on the corrosion behavior of carbon steel at 90°C," *Corrosion Science*, vol. 52, no. 6, pp. 2050–2058, Jun. 2010.
4. S. N. Smith, "Prediction of Corrosion in Slightly Sour Environments," paper No. 02241, *Corrosion/2002*, no. 02241, pp. 1–16, 2002.
5. E. Abelev, J. Sellberg, T. Ramanarayanan, and S. L. Bernasek, "Effect of H₂S on Fe corrosion in CO₂-saturated brine," *Journal of Materials Science*, vol. 44, no. 22, pp. 6167–6181, Sep. 2009.
6. Y. Choi, S. Nescic, and S. Ling, "Effect of H₂S on the CO₂ corrosion of carbon steel in acidic solutions," *Electrochimica Acta*, vol. 56, no. 4, pp. 1752–1760, 2011.
7. D. Jingen, Y. Wei, L. Xiaorong, and D. Xiaoqin, "Influence of H₂S Content on CO₂ Corrosion Behaviors of N80 Tubing Steel," *Petroleum Science and Technology*, vol. 29, no. 13, pp. 1387–1396, May 2011.
8. M. Lucio-Garcia, J. G. Gonzalez-Rodriguez, M. Casales, L. Martinez, J. G. Chacon-Nava, M. Neri-Flores, and Martinez-Villafañe, "Effect of heat treatment on H₂S corrosion of a micro-alloyed C–Mn steel," *Corrosion Science*, vol. 51, no. 10, pp. 2380–2386, Oct. 2009.
9. K. J. Lee, S. Nescic, "The Effect of Trace Amount of H₂S on CO₂ Corrosion Investigated by Using the EIS technique," no. 05630, pp. 1–16, 2005.
10. W. Sun, S. Nescic, "A Mechanistic Model of H₂S Corrosion of Mild Steel," no. 07655, pp. 1–26, 2007.
11. G. Zhang, Y. Zeng, X. P. Guo, F. Jiang, D. Y. Shi, and Z. Y. Chen, "Electrochemical corrosion behavior of carbon steel under dynamic high pressure H₂S/CO₂ environment," *Corrosion Science*, vol. 65, pp. 37–47, Dec. 2012.
12. Navabzadeh Esmaeely, S., Zhang, W., Brown, B., Singer, M., and Nescic, S., "Localized Corrosion of Mild Steel in Marginally Sour Environments", *Corrosion*, Vol. 73, No.9, pp. 1098-1106, 2017.
13. Yaakob, N., "Top of the Line Corrosion in CO₂/H₂S Environments." Electronic Thesis or Dissertation. Ohio University, 2015. OhioLINK Electronic Theses and Dissertations Center.
14. Yaakob, N., Farelas, F., Singer, M., Nešić, S., Young D., "Localized Top of the Line Corrosion in Marginally Sour Environments," *Corrosion/2016*, paper no. 7695 (Houston, TX: NACE International, 2016).
15. Navabzadeh Esmaeely, S., Zhang, W., Brown, B., Singer, M., and Nescic, S., "Localized Corrosion of Mild Steel in Marginally Sour Environments", *Corrosion/2018*, 2018.
16. Zhang, W., Brown, B., Young, D., Nescic, S., Singer, M., "Factors Influencing Localized Corrosion of Mild Steel in Marginally Sour Environments", *Corrosion/2018*, 2018.
17. S. N. Smith and M. W. Joosten, "Corrosion of Carbon Steel by H₂S in CO₂ Containing Oilfield Environments," *NACE International/2006*, vol. Paper No.0, no. 06115, pp. 1–26, 2006.
18. J. Ning, Y. Zheng, D. Young, B. Brown, S. Nescic, "Thermodynamic Study of Hydrogen Sulfide Corrosion of Mild Steel", *Corrosion*, vol.70, no.4, pp. 375-389, 2014.
19. Gao, S., Jin, P., Brown, B., Young, D., Nescic, S., and Singer, M., "Corrosion Behavior of Mild Steel in Sour Environments at Elevated Temperatures", *Corrosion*, Vol. 73, No. 8, pp. 915-926, 2017.
20. Gao, S., Jin, P., Brown, B., Young, D., Nescic, S., and Singer, M., "Effect of High Temperature on the Aqueous H₂S Corrosion of Mild Steel", *S Corrosion*, Vol. 73, pp. 1188-1191, 2017.

21. B. Brown and A. Schubert, "The Design and Development of A Large-Scale, Multiphase Flow Loop for The Study of Corrosion in Sour Gas Environments," no. 02502, pp. 1–19, 2002.
22. ASTM Standard G1, 2003, Standard Practice for Preparing, Cleaning, and Evaluating Corrosion Test Specimens, ASTM International, West Conshohocken, PA, 2003, DOI: 10.1520/G0001-03, www.astm.org.
23. ASTM G46-94(2005), Standard Guide for Examination and Evaluation of Pitting Corrosion, ASTM International, West Conshohocken, PA, 2005, www.astm.org
24. J. Morse, F. Millero, J. Cornwell, and D. Rickard, "The chemistry of the hydrogen sulfide and iron sulfide systems in natural waters," *Earth-Science Reviews*, vol. 24, no. 1, pp. 1–42, Mar. 1987.
25. M. Nordsveen and S. Nestic, "A Mechanistic Model for Carbon Dioxide Corrosion of Mild Steel in the Presence of Protective Iron Carbonate Films — Part 1 : Theory and Verification," *Corrosion*, vol. 59, no. 5, pp. 443–456, 2003.
26. IUPAC: Chemical Data Series No. 21, Stability constants of Metal-Ion Complexes. Par A: Inorganic ligands. Pergamon Press.
27. Benning, L. G., Wilkin, R. T., Barnes, H. L., "Reaction pathways in the FeS below 100C, *Chem. Geol.*, 2000, Vol.167, 25-51
28. J. Han, B. N. Brown, D. Young, and S. Nešić, "Mesh-capped probe design for direct pH measurements at an actively corroding metal surface," *Journal of Applied Electrochemistry*, vol. 40, no. 3, pp. 683–690, Dec. 2009.
29. S. Nestic, L. Lunde, "Carbon Dioxide Corrosion of Carbon Steel in Two-Phase Flow", *Corrosion*. vol. 50, no. 9, pp. 717-727. 1994.
30. B. Brown, S. Nestic, "Aspects of localized corrosion in a H₂S/CO₂ environment", in *Corrosion/2012*, paper no. 1559Conference, # C2012-0001559
31. W. Sun and S. Nešić, "Basics Revisited: Kinetics of Iron Carbonate Scale Precipitation in CO₂ Corrosion," *CORROSION/06*, paper no. 365 (Houston TX: NACE, 2006).
32. W. Sun, "Kinetics of Iron Carbonate and Iron Sulfide Scale Formation in CO₂/H₂S Corrosion," (PhD Thesis, Ohio University, 2006).